DESIGN, FABRICATION, AND QUALIFICATION OF A 3D PRINTED METAL QUADRUPED BODY: COMBINATION HYDRAULIC MANIFOLD, STRUCTURE AND MECHANICAL INTERFACE

J. T. Geating*, M. C. Wiese*, and M. F. Osborn*

*Naval Research Laboratory, DC 20375

Abstract

Additive manufacturing allows designers to make complex, efficient parts that are not achievable through conventional manufacturing techniques. Efficiencies are achieved by combining structural members, component interfaces, and hydraulic power distribution elements while eliminating redundant structural mass and volume. This paper documents the design, fabrication, inspection and testing of complex additively manufactured metal components. Parts utilizing AlSi10Mg aluminum alloy combine the roles of hydraulic manifold, mechanical interface, and core structure for a meso-scale quadruped robot. These parts allow Naval Research Laboratory (NRL) engineers to design and construct a highly capable quadruped robot that is both dynamic and lightweight. Metal parts were designed with computer aided design (CAD) and constructed using powder-bed direct laser metal sintering (DLMS). High-pressure hydraulic lines with internal fluid passageways were printed into the body assembly seamlessly creating a complex hydraulic manifold. After fabrication, a rigorous program involving post-processing, inspection, and destructive and non-destructive testing was performed to validate the design and manufacturing methods. The manifold has been approved for use and integrated on the quadruped, awaiting system level testing.

Introduction

There is current wide-spread enthusiasm for additive manufacturing (AM) technologies with a proliferation of devices leveraging the technique, as well as great anticipation for the vast potential utility and future applications. This is with good reason, as AM removes significant barriers to entry for new manufacturers, including the need for specialized knowledge, reductions in safety hazards, and lower overall cost. The printers and print materials are generally considered safe in significant contrast to traditional subtractive mill and lathe operations that require specialized training of personnel to ensure high quality and safety of operations. Although plastic AM printing has been prevalent for years now, metal AM printing has recently begun transitioning from primarily an R&D effort to production applications. Although these technologies are less accessible to the general public and significantly more expensive, metal has inherent benefits for high-strength applications. The advent of metal printing opens additional possibilities for AM applications, but also raises questions about whether the product quality is comparable to the high standards of conventional machining techniques. This paper attempts to highlight some of the experiences of researchers at the US Naval Research Laboratory (NRL) in Washington, D.C. as early adopters of metal-based AM technologies.

Background

NRL conducts a broad range of basic and applied research, and also provides systems engineering, hardware integration and program-level support to government customers for engineering prototypes of advanced systems. Research projects at NRL are competitively

awarded based on science and technology merit, and are grouped into focus areas that support the broader objectives of the Naval Science and Technology Strategy. NRL researchers seek out difficult problems for research efforts, with an emphasis on problems of high interest to the military services. Solutions to these problems provide new capabilities, improve soldier health and welfare or streamline operations. As one of these programs, NRL has been investigating advanced hydraulic actuators and controls under a five year 6.2 Discovery and Invention research effort called Meso-scale Robotic Locomotion Initiative (MeRLIn). The goals of MeRLIn are to develop hydraulic actuators and controls to enable the creation of a highly dynamic quadruped robot that can be built on a scale such that it can be carried in a soldier's backpack for deployment on demand.

The MeRLIn program is inspired by larger payload-carrying quadrupeds build by Boston Dynamics for the Defense Advanced Research Projects Agency (DARPA) over the past decade. Such robots were designed to offload backpacks of deployed soldiers, which can exceed 100 lbs, and overcome terrain too severe for wheeled platforms. Such large payload-capable robots were deployed with Marines for field exercises to demonstrate their capabilities, performance in real-world environments, and potential operational use cases. The conclusions resulting from these exercises were twofold: the robots were too big, and they were too loud. The issue with size was that these complex machines themselves required significant logistical support including specialized handling equipment, spare parts and required significant operational resources including fuel and maintenance. In essence, the large robots were both targets for our adversaries, and required their own supply chain with a burden comparable to their potential payload-carrying benefits. The second concern was noise, which emanates primarily from the internal combustion engine used as the primary power source, and the fear that such a noise source would give away troop positions. Given this feedback, the MeRLIn research team focused on maintaining all the robot's dynamic capabilities while making it small and portable enough to fit in a soldier's backpack and operating from rechargeable batteries to address the noise issue.

NRL envisions a different use case for near-term robotics, where robots perform covert or hazardous tasks rather than carry significant payloads over long distances. In these use cases, the payload is likely to be a small sensor suite providing situational awareness to the soldier. Potential robotic tasks include walking point or flank for a mobile squad, establishing and maintaining a secure autonomous perimeter for an encampment, or performing other hazardous tasks, such as clearing rooms of buildings in a contested environment, transporting supplies between soldiers under fire, performing explosive ordnance operations, or countering the threats of improvised explosive devices (IEDs). These robots are envisioned to have significant dynamic capabilities such that the robot can run faster than a typical soldier, and overcome obstacles by jumping over features such as a culvert, fallen tree, or other debris. In other applications, the significant dynamic capabilities of the robot can be traded for a less dynamic platform with a larger payload capability in the 5-10 lb range.

The key to making a small, dynamically capable robot is maintaining high system-level specific power. High specific power allows the high vehicle-level acceleration necessary for running and jumping, and may enable future capabilities such as climbing. Precursor work at NRL highlighted the inability of small electromechanical actuators to provide sufficient power at these small scales to enable the rapid joint movements required for dynamic operations. Pneumatic systems with pneumatic artificial muscles (PAMs) have also been investigated on separate programs, but a combination of low volumetric efficiency, single-action stroke, and

complex locomotive controls to overcome the compressibility of the working fluid prevented their use. As such, the MeRLIn program focused on micro-hydraulic systems to provide the power density needed for this application, and a significant focus of the program has been creating miniature actuator systems including double-acting hydraulic cylinders, legs, pumps, and then integrating them together with sensing systems. A second major thrust of the MeRLIn program is developing and implementing the real-time adaptive control systems necessary to provide responsive and stable operations at the leg and vehicle levels. These controls adapt the effective actuator compliance such that the actuator can be stiff while providing the high force-levels needed for a run or jump maneuver, and then commanding active-compliance to simulate the action of a shock-absorber on the subsequent landing within one cycle of the gait profile.

The MeRLIn program uses Additive Manufacturing in several ways. The most basic is the rapid prototyping of parts to perform fit checks and gain confidence in a parts design before committing more significant resources towards more traditional metal machining vendors for the necessary high-strength parts. One consideration is that operations at the prototype level have to take into account the lower material strength for the temporary plastic parts to ensure that they are used within their capabilities. AM parts have been used routinely as stand-in parts for items with long manufacturing lead times, or as design placeholders during system-level design iterations.

The most critical use of AM for the MeRLIn program is to maintain high power density at the system-level. AM contributes to this in two ways, the first of which is that AM allows a single part to be created that acts as a combination of two or more traditionally manufactured parts. As detailed further in the Design section, AM allows for a three part hydraulic manifold to replace multiple fluid system hoses and fittings while functioning as the mechanical structure for the robotic platform. This significantly reduces robot mass and volume by removing individual parts from the system. Additionally, AM provides another function, which is the ability to streamline the mechanical interfaces between parts. This aspect of AM allows the different functions of the robot to be positioned in extremely close proximity to each other and removes significant secondary structures, such as individual mounting interfaces and structural housings.

At the onset of the MeRLIn program, the potential benefits of using AM were fairly well established. Plastic AM parts had become ubiquitous and NRL owned and operated numerous plastic printers, primarily used for creating rapid-design prototypes. Metallic AM parts were just becoming available, either through other government agencies or procurement via commercial vendors. NRL had significant experience with metal AM printing for small mechanical parts, including novel use as fluid manifolds to create small fuel cells for unmanned aerial vehicles.[1] The hydraulic manifold discussed in this paper is the most complex and technically challenging metal AM attempted by NRL to date. The manifold design, complete with its complex internal passageways, cannot be built with traditional manufacturing techniques. Additionally, the finished part becomes an integral portion of an active high-pressure hydraulic system and is mated to valves with critically tight sliding fit tolerances that are extremely contamination sensitive. The use of micron-scale metal powders during the AM process poses a contamination risk to the valve if residuals were to remain in the part, or be released during operation. This requires the manifold to undergo post-processing to purge all remaining powder from the fluid lines. While the use of AM for such a complex part posed numerous challenges, it was viewed as an enabling technology for minimizing robot mass and volume.

As with any new technology, there were a few known issues to be resolved, some open questions to be answered, and it was recognized that both the technology and implementation had ample room to mature. The MeRLIn program attempted to address these issues in order to take advantage of the significant mass and volume reduction possible using metal AM technologies. The designs, applications, processes and findings of these investigations are summarized in the remaining sections of this paper.

Design

System Design Requirements

The MeRLIn program builds two hydraulic quadruped robot prototypes during the five year program. The first tethered prototype called 'Butch' serves as research platform for a second generation untethered robot prototype named 'Scout' that will be built starting in 2018. At the heart of 'Butch' is its AM manifold, fed power over a tether from an industrial hydraulic power unit. The design of the manifold was driven by its need to interface with numerous components, support structural loads of the quadruped, efficiently pass hydraulic power to the actuators, and minimize mass. Although it was desired to make the robot as light as possible, we initially targeted a mass of 22 lb (10 kg) to balance near term manufacturability and dynamic capability. Our target mass was based off of a systems level mass estimate, which was driven by the least scalable component, the hydraulic servo valves. Our 22 lb (10 kg) target falls within the 'mesoscale' classification, a driving goal of the MeRLIn program. This target mass was used to size the actuators, which in turn determined the flowrate requirement for the manifold to support. Pictures of the quadruped are shown in Figure 1.

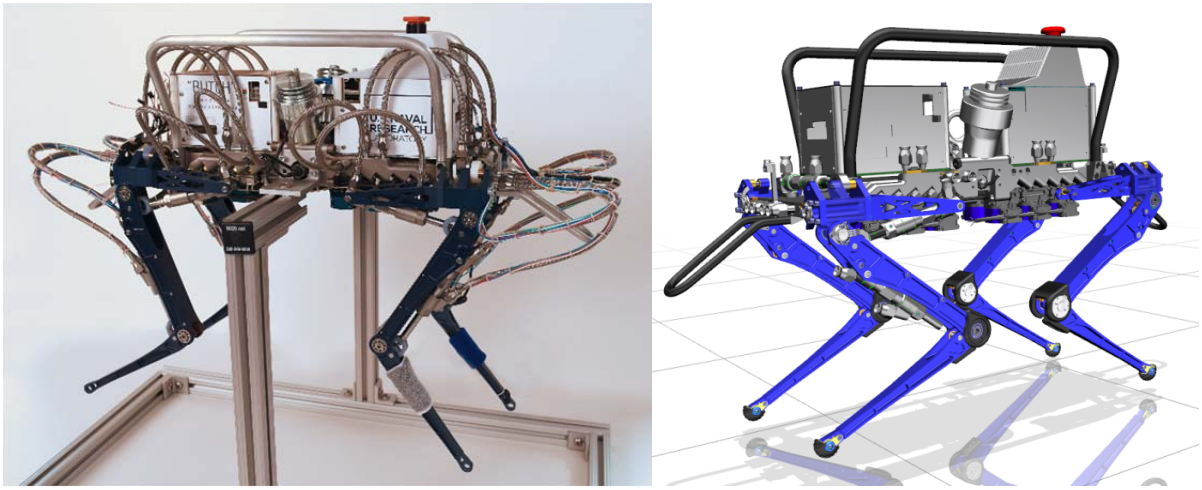

Figure 1. Photo and CAD rendering of the hydraulic quadruped, *Butch*.

System pressure was set to the industrial hydraulic standard rating of 3000 psi. Exceeding this pressure would prevent the use of many COTS hydraulic components, both on the quadruped and for the off-board hydraulic power unit. At the same time, reducing system pressure would restrict system power density and decrease mobility.

Interface and General Design

To ensure the manifold could interface with all required subsystems, we first decided on driving components. The most significant driving components were the valves, accumulators, and actuators - the valves and accumulators because of their large volume and predetermined

interfaces, and the actuators because of their restrictive location requirements to maintain leg strength and range of motion. Parts were iteratively located in different configurations until the most viable concept was determined. From there, smaller and more customizable components were added to the system until a detailed design was reached. During this process, the footprint of the electronics board was selected, driven by both the packaging of Butch, as well as the footprint of the onboard COTS microprocessor. The components the manifold was required to interface with are listed in Table 1.

Table 1. Components interfacing with manifold

Component	Functionality	Vendor	Part description
Hydraulic Tether	Provides hydraulic power	Goodridge	600 series tubing, 04 size
Micro accumulators	Provides high instantaneous hydraulic power in excess of pump flowrate	Hawe	ACS/13
Subminiature valves	Controls hydraulic actuators	Moog	EO24 (custom two stage flow gain)
Actuator hydraulic lines	Connects manifold to actuators	Goodridge	600 series tubing, 02 size
Pressure transducers	Provides system input and return pressure, and up to three DOFs of cylinder pressure	Meggitt	8510B-2000-DM1
Electronics boxes	Houses NI SOM, as well as all analog and digital I/O. Custom in-house design	In-house (NRL), National Instruments	N/A
Inertial Measurement Unit	Used for state estimation	Lord Microstrain	3DM-GX4-25
Carrying handles/fall guards	For lifting quadruped, as well as protecting from falls	In-house (NRL)	N/A
Legs	For locomotion	In-house (NRL)	N/A
Hydraulic actuators	For moving leg joints	In-house (NRL)	N/A

Detailed design

We used an iterative routing process to connect the valves to the input pressure and cylinder outputs. The leg mechanical mounts were designed to preserve as much range of motion as practical, and the other interfaces were fit around each other in a puzzle-like fashion. A three-part design was decided on, with two identical front and hind body manifolds, and one central interface manifold. This allowed for a good deal of modularity, ease of assembly, manufacturability, and flexibility to fit within the build volume of commercially accessible metal printers. In total, there are 32 discreet fluid lines between the three manifolds as shown in Figure 2 and 3.

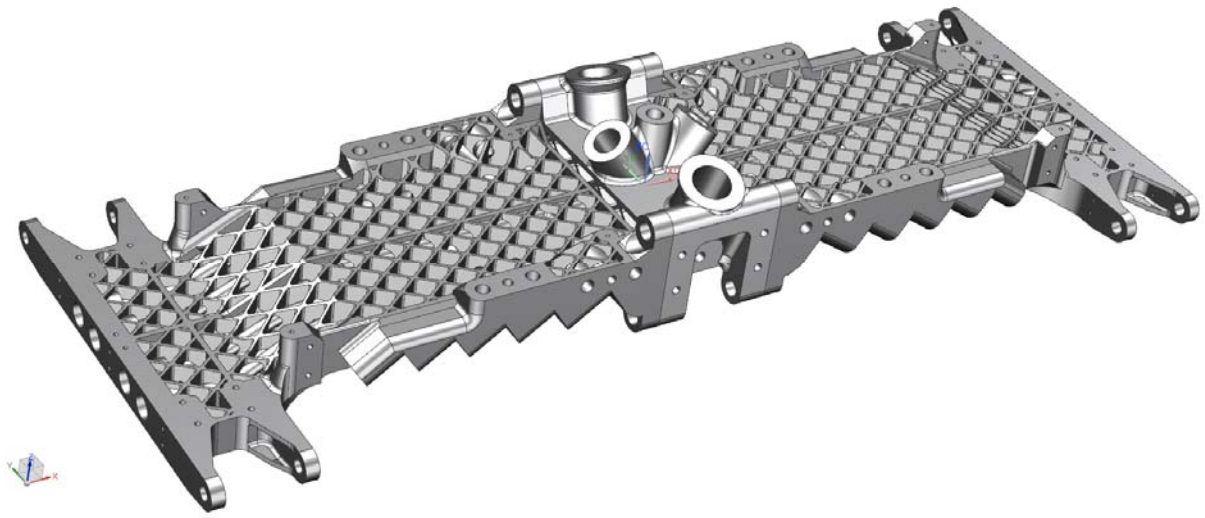

Figure 2. Three-part manifold assembly

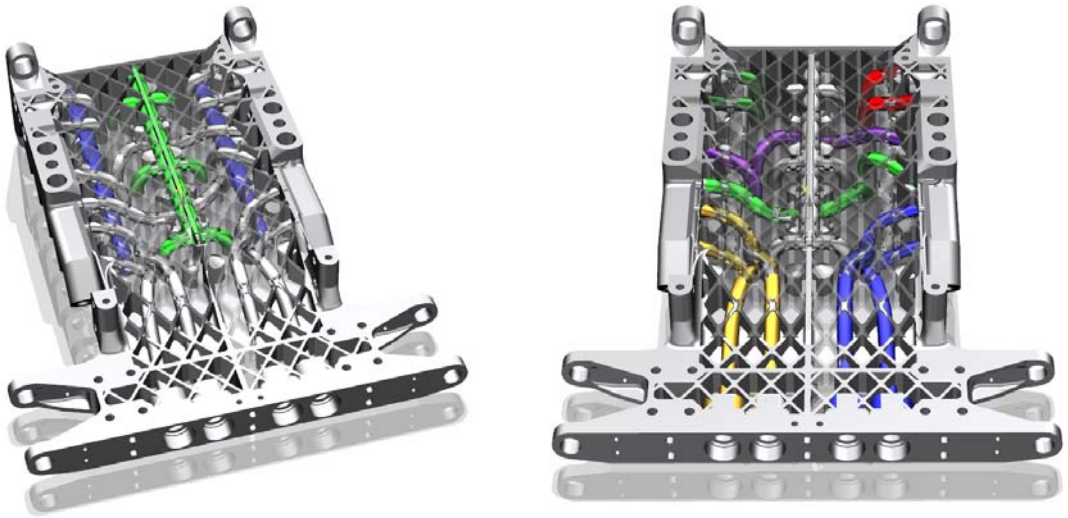

Figure 3. Colored supply and return lines, green and blue resp. (left), actuator lines, color indicates one actuator (right)

To size the integral fluid interconnects within the manifold, both the flow rate and pressure are taken into account. Based off of the desire for a highly agile system, the valves are designed for a maximum flowrate of 0.7 gpm. This flowrate was used to size the cross sectional area of the fluid interconnects using equation[2]

$$\Delta p = 2.15\times10^{-4}\,\frac{f\rho L Q^2}{d^5} \tag{1}$$

where Δp is the pressure drop across the fluid line in psi, ρ is the density of the fluid in lb/ft^3, L is the length of the fluid line in feet, Q is the flow rate in gpm, and d is the diameter of the fluid line in inches. The friction factor, f, is given by the Blasius correlation[2],

$$f = 0.316\,\mathrm{Re}^{-1/4} \tag{2}$$

$$\mathrm{Re} = 3162\,\frac{Q}{\mu d} \tag{3}$$

where Re is the Reynolds number and μ is the viscosity of the fluid. Combining Equations (2) and (3) into (1). Diameter was chosen not to exceed a pressure drop of 150 psi at maximum flowrate, or 5% of the system pressure. This resulted in internal passages of 0.06 to 0.12 inches, depending on the location in the manifold.

The designed wall thickness of the fluid passages is calculated using the nominal system pressure of 3000 psi, and the Von Mises distortion energy theory.

$$\sigma_t = \frac{r_i^2 p_i}{r_o^2 - r_i^2}\left(1 + \frac{r_o^2}{r^2}\right) \tag{4}$$

$$\sigma_r = \frac{r_i^2 p_i}{r_o^2 - r_i^2}\left(1 - \frac{r_o^2}{r^2}\right) \tag{5}$$

$$\sigma_l = \frac{r_i^2 p_i}{r_o^2 - r_i^2} \tag{6}$$

$$\sigma_v = \sqrt{\frac{(\sigma_1 - \sigma_2)^2 + (\sigma_2 - \sigma_3)^2 + (\sigma_3 - \sigma_1)^2}{2}} \tag{7}$$

In the above equations, σ_t is the tangential stress, σ_r is the radial stress, and σ_l is the longitudinal stress, correlating to principal stresses σ_1, σ_2, and σ_3, respectively, σ_v is the Von Mises stress, r_i is the tube inner radius, r_o is the tube outer radius, p_i is the internal pressure, and r is the point at which the stress is measured (r_o in this case). This results in a wall thicknesses ranging from .04" (1.0mm) for the actuators to 0.07" (1.8mm) for the system pressure line. The actuator lines had the lowest factor of safety with a maximum Von Mises stress of 8.2 ksi. This correlates to a 4.1:1 safety factor over the published yield of 34 ksi, and 6.7:1 over ultimate strength.[3]

Because commercially available hose interconnects were mass and volume prohibitive, custom fittings were developed. We developed a miniature conventional plug-in fitting for the hip adduction/abduction and hip flexion/extension joints as shown in Figure 4. For the knee joint port, we added a radial contact ball bearing to allow free rotation of the fitting as the leg moves under pressure. This was implemented due to the large relative motion of the knee actuator, inducing rotation at its port. The o-rings of this fitting seal directly against the machined aluminum ports of the manifold, although adding a stainless steel insert for better wear and life was also considered.

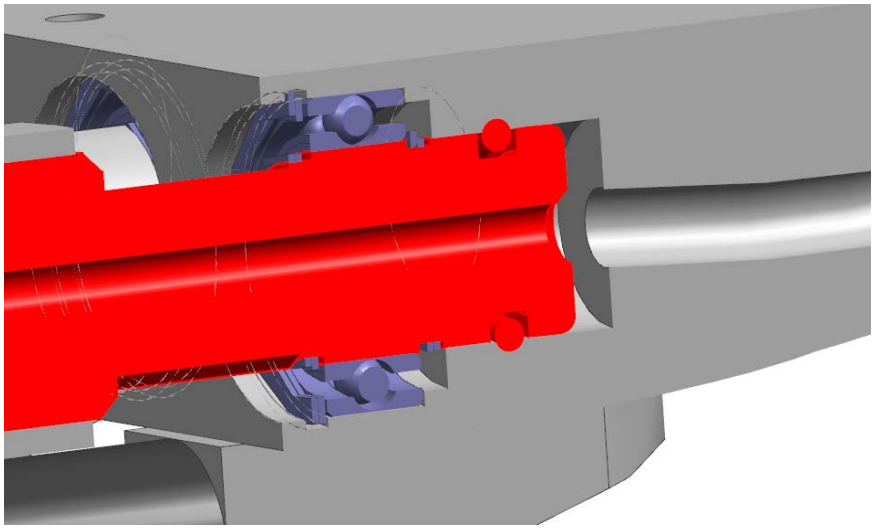

Figure 4. Section view of custom rotary plug-in fittings

The manifolds were modelled in UG NX 10.0 and exported to vendors as .stl files. The internal piping of the manifolds was modelled using spline paths with boundary conditions matching the ports. Spline parameters were visually adjusted, and measurements were taken to verify wall thickness was preserved between nearby passageways. In parallel, we generated a solid exceeding the dimensions of the manifold with a diamond pattern of lightening voids. Then, through a series of combining solid models, performing add/subtract/intersection Boolean operations, and offsetting faces, the diamond pattern replaced much of the volume of the manifold.

The only portions of the manifold that were kept solid were the walls of the tubes, a given thickness around any machined features, and several structural ribs and walls to react global loads. This process was especially prone to Boolean errors as offset faces intersected in unstable scenarios. In its most extreme case, the wall thickness of several passageways were left aggressively low, just above a 4:1 burst ratio, because increasing them further caused errors in the model. It is unknown if other CAD packages would have handled this series of Boolean operations with more ease. Another option was to use a third party program intended for the triangulated files 3D printers use (.STL's), as these programs give numerous infill options. This option was avoided, as many of the light-weighting features closely reference other features across the manifold. Triangulating the model (i.e. no longer knowing that a cylinder is a cylinder, but instead a surface made of triangles) would have prevented creating many of the precise rib and offset features important for efficient structural loading.

Figure 5 shows several steps of the manifold light-weighting process.

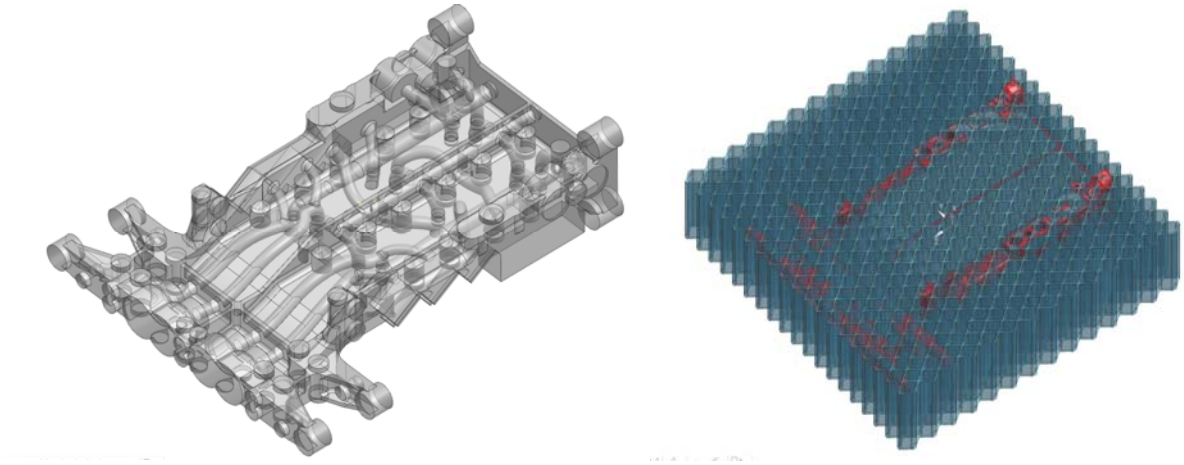

Figure 5. Primary machine features (left), and diamond mesh pattern fill (right).

The progression of manifold mass as the design matured and was light-weighted is shown in Table 2. The light-weighted version 2 is the manifold discussed in this paper.

Table 2. Progression of manifold mass reduction

Version	Body Manifold (g)	Center Manifold (g)
Version 1, solid	595*	273*
Version 1, light-weighted (Stratasys)	451	139*
Version 2, solid	406*	174*
Version 2, light-weighted (Xometry)	256	131

*Only designed in CAD, not printed

Between the three parts, this resulted in 114 fluid connections and 162 mechanical features (e.g. threaded holes).

Table 3. Overview of manifold mechanical and hydraulic interfaces.

Description	Type	Part Quantity	Features
Body Manifold (quantity 2 per quadruped)			
Pressure/return lines to center manifold	Hydraulic	N/A	3
Valve ports	Hydraulic	6	24
A/B hose connections	Hydraulic	12	12
Pressure transducer ports	Hydraulic	12	12
Center manifold mechanical interface	Mechanical	N/A	4
Valve mechanical interface	Mechanical	N/A	24
Electronics box mechanical interface	Mechanical	1	4
Retaining plate mechanical interface	Mechanical	4	4
Handle mechanical interface	Mechanical	1	4
HAA actuator mechanical interface	Mechanical	2	8
Leg mechanical interface	Mechanical	2	4
HAA hardstop mounts	Mechanical	4	8
Future attachment mounts	Mechanical	N/A	6
Front fallguard mechanical interface	Mechanical	1	4
Cable guide mechanical interface	Mechanical	1	2
	Total Hydraulic		51
	Total Mechanical		72

Center Manifold			
P/T input	Hydraulic	2	2
Accumulator connections	Hydraulic	2	2
P/T outlets	Hydraulic	N/A	6
Pressure transducer ports	Hydraulic	2	2
Body manifold connections	Mechanical	N/A	8
IMU mount	Mechanical	1	2
Future mounting locations	Mechanical	N/A	8
	Total Hydraulic		12
	Total Mechanical		18
	Subtotal Hydraulic	114	
	Subtotal Mechanical	162	

Figure 6 shows the manifold mated to all immediately contacting components.

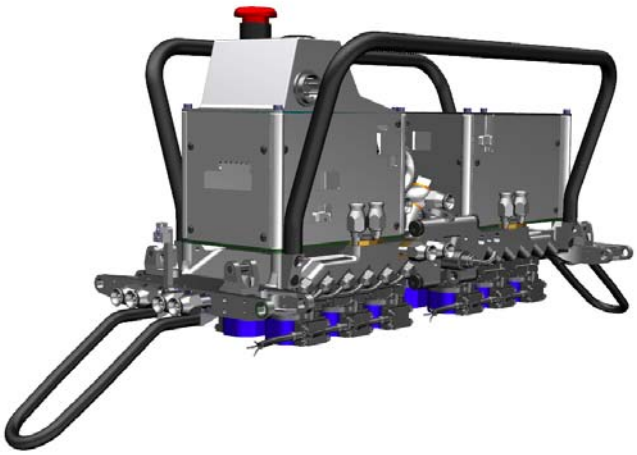

Figure 6. Manifold with directly mounted components

Fabrication

Material

An aluminum alloy (AlSi10Mg) was selected for its low density and high strength to weight ratio. Because of many of the features on the manifold were already at the minimum recommended feature size, going to stronger, denser materials and decreasing volume proportionally was not an option consistent with our minimum mass design.

AM Process

The first iteration of manifold design was printed out of house by Stratasys Direct.[4] This design was used for a single leg testbed, a developmental testbed at NRL that provides hydraulic services and controls for a two or three degree-of-freedom leg. This was a risk reduction effort prior to designing and building the full quadruped. This design was stronger and less aggressively light-weighted than the target design, and weighed 451g. The second iteration

manifold and focus of this paper was manufactured by Xometry[5], weighing 256g. The diamond light-weighting structure and internal manifold ports made this is one of the most complex DLMS parts manufactured by Xometry. Feedback was given by Xometry that we would need to add walls to several areas that would not be self-supporting during the build process; this change was implemented at NRL. An angled build orientation is shown in Figure 7, as selected by Xometry in order to minimize lengths of unsupported structure. Xometry added additional support to all overhangs, but excluded doing so for most of the diamond lattice as the support material would be inaccessible for removal. This, however, incurred risk for the printing defects. For post-processing the gross finished geometry, support material is cut away using a wire EDM, then polished by hand or milled.

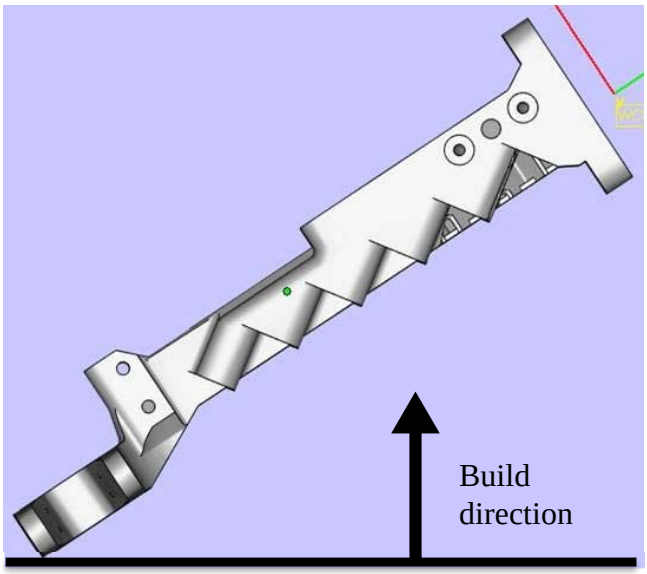

Figure 7. Orientation of the manifold in the build tray

In order to manufacture the manifold, additional material was added at all features that required post machining. These include all threaded features, precision sealing surfaces, and bearing pockets. For all surfaces requiring post machining, .02-.06 inches of material was added, with more material added for larger features.

Post processing

All post-process machining was done in-house on a Bridgeport EZ-Trak vertical mill. Features were located by inserting pins into hole features and machining locally. Because the tolerance of DLMS parts linearly increases with distance, features were re-indicated when more than 1-2 inches from each other in order to realign the machine frame with the actual location of the printed features. It was found that features deviated several hundredths of an inch from their nominal position at these distances. These finding were consistent with published vendor design guidelines, but highlight the fact that maintaining close absolute position tolerances over the span of larger AM parts remains a challenge.

In order to reduce frictional flow losses within the manifold, and more so to reduce debris creation during hydraulic operation, the internal passageways of the manifold were extrusion honed. Extrusion honing is a process in which an abrasive slurry (similar to toothpaste in

consistency) is pushed through a fluid passageway to polish the internal surfaces. To prevent critical surfaces from being abraded during this process, only a select few machining operations to connect the slurry lines were performed prior to extrusion honing. Extrusion honing was performed by Extrude Hone AFM.[6]

After receiving the manifold parts from extrusion honing, the remaining machining operations were completed. A rough cleaning was completed with soap and water using an ultrasonic cleaner. Parts were flushed with clean water to remove lose particulates, and then excess water was removed using compressed nitrogen gas. Isopropyl alcohol was flushed through all the ports, blind holes and crevices and then removed with compressed nitrogen gas. Afterwards, the parts were precision cleaned in a Forward Technology vapor degreaser using 3M Novec HFE-7100 solvent in a cleanroom where each port and passageway was flushed with solvent using either port attachment fittings or a small section of 1/16 inch Teflon tubing to get inside each passageway.

Inspection

Upon coarse visual inspection, a handful of defects and artifacts from the AM process were identified. The main defects were portions of the internal manifold piping with material either caved in or simply missing. An example of this type of defect can be seen below in Figure 8 which looks like a scoop has been taken out of the pipe wall. This discovery raised the question of whether the pipe wall thickness remained constant or the pipe internal cross sectional area was affected. If the wall thickness decreases, then mechanical stress within the wall from the hydraulic pressure increases and creates a stress concentration and structural weakness at these points. If the flow area of the pipe decreases, this would reduce flow rates. We determined that only computerized tomography (CT) scanning technology could investigate these issues nondestructively.

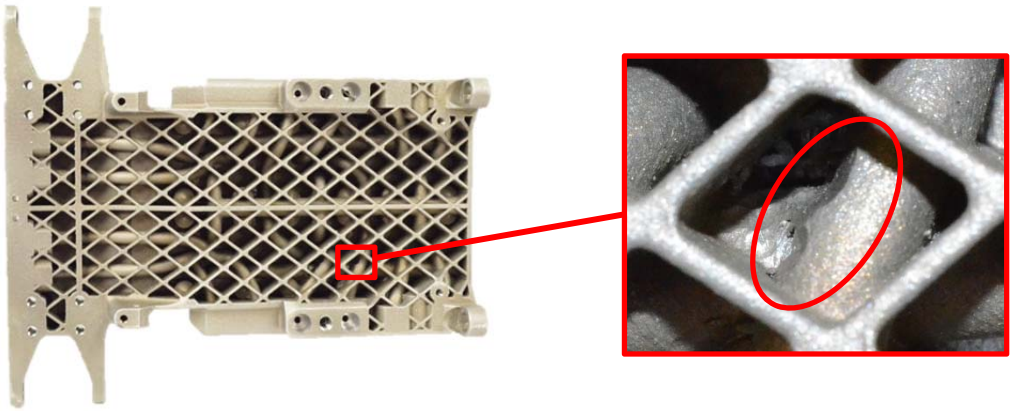

Figure 8. Inspection and imaging of manifold pipe defect.

In addition to these defects, the main artifacts found appear to be exposed support structure from the build process. An example of these artifacts is shown in Figure 9**.** Since these artifacts were in difficult-to-reach crevices within the manifold's geometry, they could not be investigated nondestructively without the use of computerized tomography (CT) scanning technology.

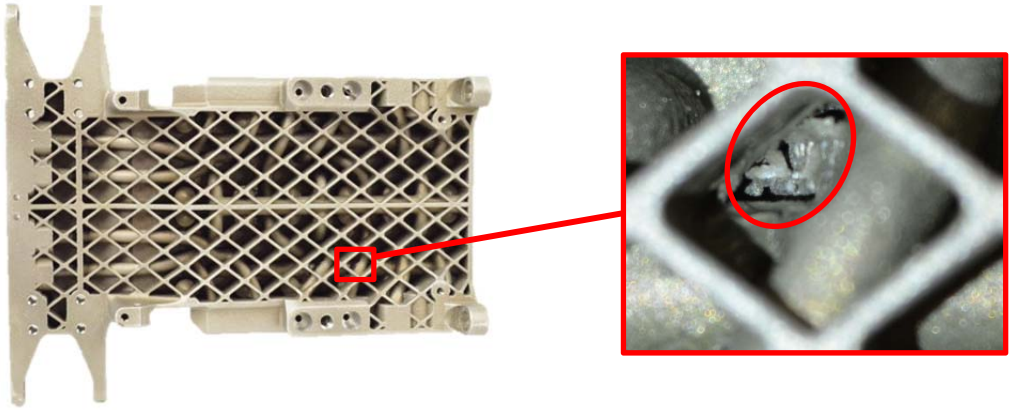

Figure 9. Example of artifacts left from the fabrication process

CT scanning technology was performed at MQC Labs in Aberdeen, Maryland in order to further investigate these issues non-destructively.[7] X-ray CT scanning refers to taking X-ray measurements from multiple orientations to produce cross-sectional or tomographic images. These images, or slices, are then stacked together to create a digital three dimensional model of the part. This process was performed on four body manifolds, two center manifolds, as well as two earlier design versions of the body manifolds. MQC Labs designed the inspection method including how the part was mounted to the rotating pedestal to capture the full part geometry, and used their experience and a number of exposure trials to match the part thickness and density with x-ray exposure to achieve the contrast and resolution needed for close tolerance inspection.

The results of the CT scans confirmed that the pipe inside cross sectional area remained constant, and that the wall thickness had significant decreases in the defect areas. This conclusion was made by first inspecting the digital three dimensional composite of the part recreated from the CT scans. Once the area of interest is defined, the individual CT scanned layer can be extracted from the model and measured at high resolution using the built in measuring tools included in the efX-CT CT analysis software.[8] Figure 10 shows an example of each of the two image types. The cross section shown indicates that most of the outside diameter of the pipe is .19" (4.6 mm), the inside diameter is .09" (2.2mm), and the wall thickness is about .05" (1.2mm). At the point of the defect, this wall thickness is .015" (0.4mm), a 60% decrease. The same area was analyzed on the other three body manifolds of the same design, with results detailed in Table 4**.** It is to be noted that the boundary of the cross section in Figure 10 below is visibly hazy. To account for this, the measurements from the efX-CT software were assumed to be accurate to 0.1 millimeter.

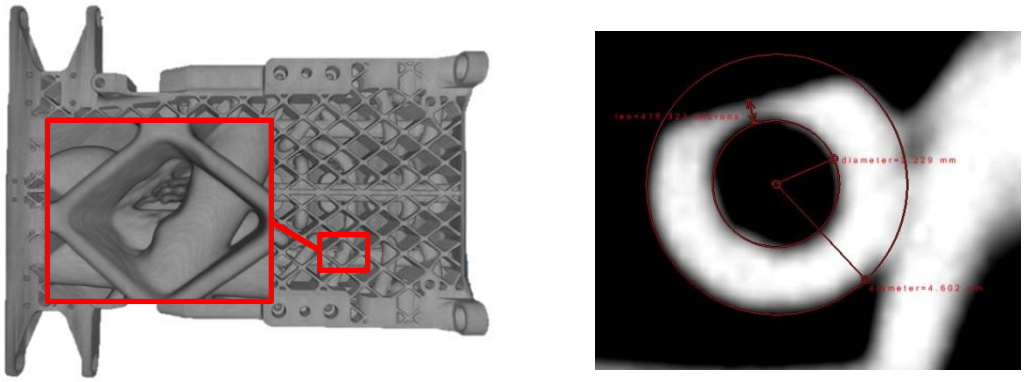

Figure 10. 3D composite created from multiple CT scans (*left*), and an x-ray image of a layer of the cross section (*right)*

Table 4. Measurements of internal piping at defect area.

Manifold Number	Outer Diameter (mm)	Inner Diameter (mm)	Wall Thickness (mm)	Wall Thickness at Defect (mm)	Wall Thickness Decrease
Part 3	4.9	2.0	1.5	0.6	61%
Part 4	4.6	2.1	1.2	0.8	37%
Part 5	4.6	2.2	1.2	0.4	64%
Part 6	4.6	2.2	1.2	0.5	59%

At the thinnest section, this would theoretically result in a Von Mises stress of 11.2 ksi, or a factor of safety of 3.0:1 over yield. There is a 5.0:1 FOS over the material's ultimate stress, resulting in a theoretical burst pressure of 14.7 ksi. However, because it is not a uniform cross section, but tapers down to this thickness at one local minimum, the actual burst pressure may be in excess of this.

A similar section was anaylzed on a previous design iteration manufactured by Stratasys Direct, as shown below in Figure 11. In this part, there were no major defects present, but the wall thickness is greater than the original part design resulting in a minor reduction in flow area of the pipe. The bulkier mechanical design of the previous design may have had a positive effect to support the piping during printing, or there could have been different AM conditions or processes between the two prints. Although the differences between these prints is out of the scope of this paper, it would be interesting to have a broader correlation between mechanical design, support material, printer conditions, and the quality of prints for complex build geometries.

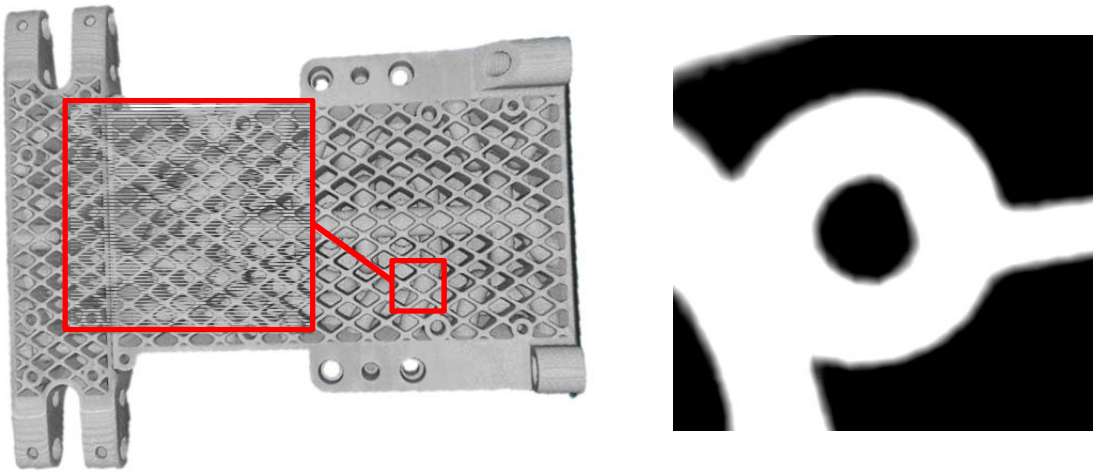

Figure 11. Example 3D composite (*left*) and CT layer image (*right*) without defects.

A detailed inspection was also performed of the center manifold parts that connect the two body manifolds together to form the structure of the quadruped as shown in Figure 12. The CT scanning data confirmed that the artifacts in the Xometry parts are exposed support material from the build process. By parsing through the solid layer by layer, a clear grid structure emerges in the void areas of the original part design. We understood that Xometry would need to add

support structure to the design such that the part could be successfully built, and the geometrical grid pattern in the CT scan confirms its use as shown in Figure 9

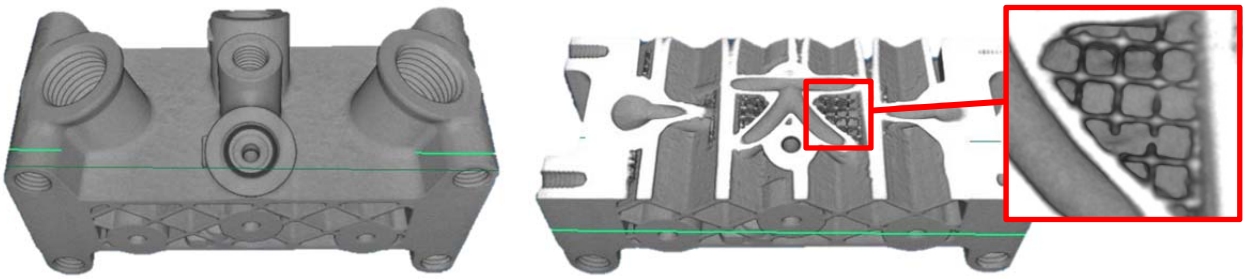

Figure 12. 3D composite CT scan (*left*), and x-ray cross sectional layer (*right*).

In terms of model accuracy, the same section detailed in Figure 10 and Table 4 was compared with the engineering model below in Figure 13 and Table 5. The differences between the four manifolds and the engineering model dimensions ranged between 4% to over 30%, or in terms of physical dimensions, from 0.007" to 0.018" difference. As detailed in the fabrication section of this paper, a significant amount of post-machining work was needed for these manifolds; however the internal piping could not be modified or measured due to the complex geometry. Aside from extrusion honing, the internal piping must be largely left untouched. CT scanning data is the only non-destructive method to comprehensively inspect the AM part's as-built internal geometry relative to the engineering design.

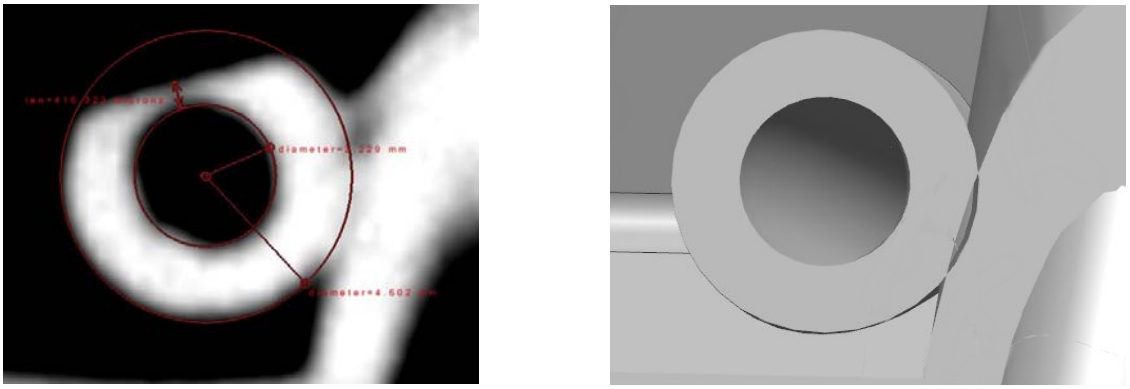

Figure 13. CT scan cross section (*left*), and designed CAD model (*right*).

Table 5. Internal piping dimensions of AM part vs. CAD model

Manifold Number	Outside Diameter (mm)	Inside Diameter (mm)	Wall Thickness (mm)	Wall Thickness Deviation (%)
CAD Model	***4.41***	***2.38***	***1.02***	***0%***
Part 3	4.9	2.0	1.5	+36%
Part 4	4.6	2.1	1.2	+20%
Part 5	4.6	2.2	1.2	+15%
Part 6	4.6	2.2	1.2	+17%

Burst Testing

The CT scan results of the defect areas for the Xometry parts confirmed pipe wall thickness reductions from the original part design which will result in high stress concentrations at these sections of the piping, and reduced safety margins. To experimentally assess the structural integrity of the manifold assembly, one of the four manifolds parts was pressure tested to failure to confirm the safety of using the AM manifolds at high pressure near humans. The experimental burst test setup is illustrated in Figure 14. It included a high pressure pump leading to a pressure gauge, then through to an isolated testing burst area where the high pressure line was connected to the manifold with other ports plugged via hoses or threaded bolts to hold pressure. A video camera was set both inside the burst chamber to record the manifold's failure mode, and outside the chamber facing the pressure gauge to document the precise pressure at failure.

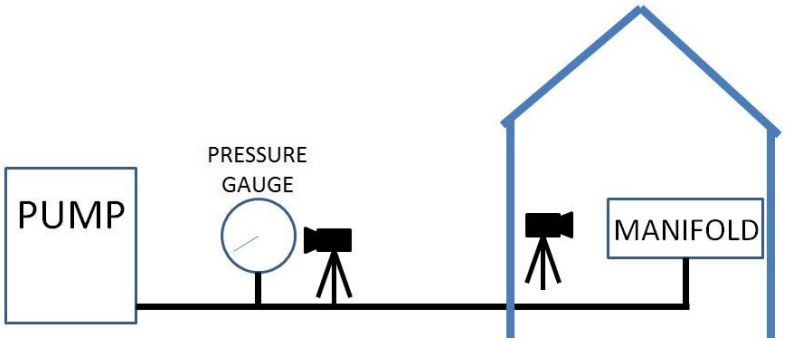

Figure 14. Proof test experimental setup. Blue structure indicates secluded burst area.

Five separate pressure tests were performed on the same manifold over the course of a single day, fixing observed failure modes along the way. The ideal target pressure was 12,000 psi, four times the maximum normal operating pressure of 3,000 psi, in order to prove safe use in close proximity to humans. Through the five trials, the maximum pressure achieved was 11,000 psi with all failure modes located at the connection points to the manifold or other hardware failures due to the experimental setup, not the manifold itself. A breakdown of the failure modes and maximum pressures held at each trial can be seen below in Table 6.

Table 6. Body manifold burst test results

Test Trial	Maximum Pressure	Failure Mode
1	8,600	Hex bolt o-ring
2	8,400	Loose hose threading
3	9,100	Retaining ring
4	11,000	Manifold adapter o-ring
5	10,500	Burst hose

The burst test unit contained the defect that resulted in the minimum pipe wall thickness as determined by visual inspection and later confirmed by CT scanning. The burst test results are considered the bounding worst case for the lot with the remaining manifolds expected to have higher pressure capabilities. The two manifolds with the thickest walls are currently installed on Butch, with the third reserved as a spare.

Figure 15 below shows a frame from the video during burst test trial number five immediately prior to failure. In all tests there was significant leaking above 8,000 psi from the experimental fixturing replacing the valves. This hindered the ability to test past 11,000 without

a more powerful pump. Despite not reaching the 12,000 psi goal, the results were deemed successful because the manifold held up hydraulically over the course of five tests, including two tests over 10,000 psi. There was one failure not caused by the experimental setup (trial 3), the retaining ring for the rotary plugin fitting sheared through its port at 9,100 psi. However, the geometry of this port allowed modification of the remaining manifolds which had not been post-machined yet, theoretically doubling their strength. The ports of the failed unit were tapped and plugged to allow subsequent testing.

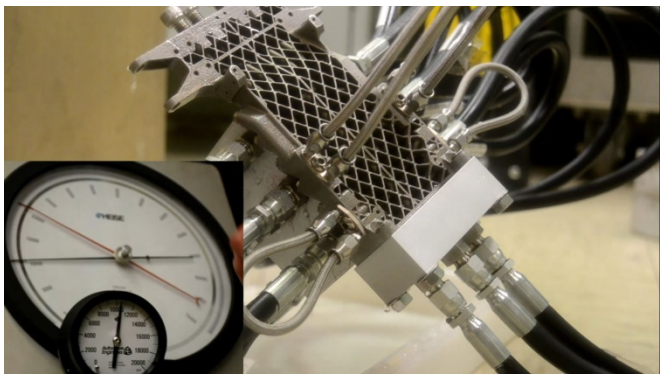

Figure 15. Still frame of burst test #5 prior to failure.

Fatigue Analysis

Fatigue analysis was performed to estimate the fatigue life of the manifold pipe with the defect relative to the nominal wall thickness. Most of the required material properties had already been experimentally found for sintered AlSi10Mg,[10,12] except for the Paris Equation constant, *C*, for which solid Aluminum 6061-T651 properties were used as a conservative estimate.[11] First the calculation was performed using the defect wall thickness of the engineering model with a semicircular initial crack, outlined in Figure 16.[9-12]

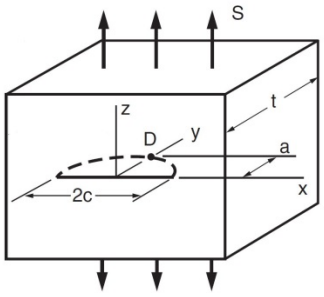

Figure 16. Semicircular initial crack geometry in a thick-walled cylinder[9]

Assuming a thin-walled pipe, the hoop stress, σ_h, is defined as[13]

$$\sigma_h = p_{\max}\left(\frac{\left(r_o/r_i\right)^2+1}{\left(r_o/r_i\right)^2-1}\right) \tag{8}$$

where p_{max} is the maximum fluid pressure. With inner and outer radii of 0.0469 inches and 0.0626 inches, respectively, and assuming a fluid pressure of 3000 psi, this yields a hoop stress of 10.66 ksi.

According to the Paris-Erdogen Law,

$$K = Y\sigma_h\sqrt{\pi a} \tag{9}$$

where K is the stress concentration, Y is the geometric factor (conservatively estimated to be equal to unity),[9] and a is the depth of the crack. Assuming that the value of the stress concentration at failure, K_{IC}, is equal to 36.4 ksi, this yields the crack length at failure, a_f,

$$\begin{aligned} K_{IC} &= Y\sigma_h\sqrt{\pi a_f} = 36.4\,[ksi\sqrt{in}] \\ a_f &= 3.711\,[in] \end{aligned} \tag{10}$$

Since a_f is greater than the thickness of the pipe at 0.0157 inches, we set the crack length at failure to that. From there, the growth rate of the crack per cycle number, N, is given by

$$\frac{da}{dN} = C\Delta K^m = C\left(Y\Delta\sigma\sqrt{\pi a}\right)^m \tag{11}$$

where C is the Paris equation constant for Al 6061-T651, and m is assumed to have a value of 4. Integrating the crack length, a, from the initial value to the thickness of the tube yields the fatigue life of the component.

$$\begin{aligned} N_f &= \int_{a_i}^{a_f} \frac{da}{CY^m\Delta\sigma\left(\pi a\right)^{\frac{m}{2}}} \\ &= \int_{0.00984}^{0.0157} \frac{da}{\left(1.604\times10^{-10}\right)\left(10.66\right)^4\left(\pi a\right)^2} \\ &= 1.855\times10^6 \text{ cycles} \end{aligned} \tag{12}$$

The same process above was performed for the nominal pipe wall thickness, yielding 58 million cycles required for the pipe to fail. Therefore, nominal to defect wall thickness is a reduction in an order of magnitude; however, 1.8 million cycles is still above the intended scope for this vehicle. If the cyclic pressure was increased from 3,000 psi to 4,500 psi in the worst case thin walled pipe scenario, the amount of cycles would decrease from 1.85 million to 360,000 cycles.

Conclusions

The MeRLIn program created unique high-performance hydraulic manifolds that performed multiple design functions using metal AM techniques. Although the quadruped has not yet been fully pressurized and actuated, all the individual components have been successfully tested. Despite the flaws that we identified visually and characterized through CT scanning, these parts have been deemed acceptable for use in a research and development environment. Both the

analytical and experimental burst pressures exceed 3.5:1, but it remains concerning that such a large amount of material is missing. The parts were designed to exceed a 4:1 safety factor over yield stress, and now there is only a theoretical 3:1 margin over yield and 5:1 over burst (for the worst case manifold). However, because a failure in a defect area is expected to be relatively non-violent, easily noticeable, and the area is protected by mounted components, the part will be put into limited use. After fatigue analysis, the defect areas are expected to withstand roughly 1,800,000 cycles, an order of magnitude smaller than the non-defect areas but still above the scope of intended use.

The most significant lesson learned was the susceptibility of 3d printing to complex, unsupported geometry. Xometry's leading hypothesis for the cause of the defect is that the lattice structure resulted in irregularities in heat exposure, causing local hot and cold spots, especially in layers farther from the print bed. When unsupported structure is sintered far away from the supporting lattice, the laser is less effective, resulting in 'crunchy' non-structural material which is prone to removal during the cleaning process. This is compounded by the fact that the powder does not fully sinter during the first pass the laser takes, but finishes sintering over subsequent laser passes. When unsupported geometry is introduced, fresh powder does not have already sintered powder nearby and is prone to failed sintering. However, this is purely speculative and the root cause is still unknown.

NRL was mostly out of the loop in deciding where Xometry added support material to the build file. In the future – and in retrospect – we would work more closely with the 3D printing company or operators to identify all areas of concern and add additional support material where appropriate. Had we known the risk of performance-degrading defects, we would have undoubtedly done this. Unfortunately, this would be a very time consuming process due to the large number of unique tubular features across the diamond lattice structure. For modeling support material, it would not be recommended to use engineering CAD software, even though the opposite was recommended for generating desired part geometry. This task would be better suited to dedicated 3D printing software that contains all of the printer build constraints.

This program answered basic questions about the applicability of metal AM to create challenging high-performance parts. The results of the MeRLIn program help us understand what the AM technologies can and can't do, where the technology is well suited as well as where it is poorly suited, and where additional margins and constraints should be applied for future similar efforts. Future manifold builds for the MeRLIn program, including those for the second generation 'Scout' robot, will build on the lessons learned through this metal AM experience.

AM technology has changed the way we do research at NRL. Scientists use the rapid prototyping capabilities to perform quick design builds to compare alternative approaches or reduce risk that lead to better products or experiments. The rapid turnaround times for manufacturing using these tools allow for broader fields of inquiry than the traditional manufacturing approaches that required detailed design drawings and more expensive parts. These tools allow for faster iteration and more thorough experimentation and results.

References:

[1]Swider-Lyons, K., "3-D Printing in Hydrogen Fuel Cells for Unmanned Systems", *Spectra, An Official Publication of the Naval Research Laboratory*, 2014.

[2]Stratasys Direct Manufacturing, "Aluminum AlSi10Mg Direct Metal Laser Sintering Material Specifications," 2015.

[3]Extrude Hone AFM. *Extrude Hone AFM – Abrasive Flow Machining.* [online] Available at: http://www.extrudehoneafm.com/ 2017.

[4]Stratasys Direct Manufacturing. *Stratasys Direct Manufacturing. [online]* Available at: https://www.stratasysdirect.com/ 2017.

[5]Xometry.com. *CNC Machining Services & 3D Printing Services – Xometry.* [online] Available at: https://www.xometry.com/ 2017.

[6]Munson,B.,Okiishi,T. and Young, D. *Fundamentals of Fluid Mechanics.* New York: Wiley. 1999.

[7]MQC Labs: *Cutting edge technology equipment. Exceptionally trained inspection personnel.* [online] MQClabs.com. Available at http://mqclabs.com/ 2017.

[8]EFX-CT 4nsi.com. *3D Computed Tomography Software, North Star Imaging*. [online] Available at: https://4nsi.com/software/efx-ct/ 2017.

[9]Dowling, N. E. Mechanical behavior of materials: Engineering methods for deformation, fracture, and fatigue. Boston: Pearson. 2013.

[10]Tang, Ming, "Inclusions, Porosity, and Fatigue of AlSi10Mg Parts Produced by Selective Laser Melting" Dissertations. 903. 2017.

[11]Ribeiro, A., Jesus, A. and Fernandes, A. FATIGUE CRACK PROPAGATION RATES OF THE ALUMINIUM ALLOY 6061-T651. Proceedings of COBEM [online]. 2005.

[12]Hitzler, L., Hirsch, J., Schanz, J., Heine, B., Merkel, M., Hall, W. and Öchsner, A. "Fracture toughness of selective laser melted AlSi10Mg". Proceedings of the Institution of Mechanical Engineers, Part L: Journal of Materials: Design and Applications, 2017.

[13]Plymouth University, Fose1.plymouth.ac.uk. *Pipe Pressure Surges.* [online]